Influence of Intake Valve Structure Combined with Valve Lift Dissimilitude on Intake Performance of Diesel Engine

W. Zhang, W. D. Jian, Z. H. Chen[†], Z. H. Li, L. P. Meng, L. B. Xie and X. Y. Zhang

Yunnan Key Laboratory of Internal Combustion Engine, Kunming University of Science and Technology, Kunming 650500, China

†*Corresponding Author Email: chenzhaohuiok@sina.com*

ABSTRACT

For diesel engines equipped with a combined spiral/tangential inlet, the main object of the valve structure and valve lift dissimilitude strategies is the valve, the changes of both will alter the motion state of the in-cylinder airflow, which has an important impact on the formation and combustion of the mixture. In order to investigate the flow performance of valve structure and valve lift dissimilitude, this paper used computational fluid dynamics (CFD) numerical simulation and multi-parameter regression methods to optimize the dual intake valve structure and obtained three valve structures with better intake performance first. Then, the optimized intake valve structure models were combined with the valve lift dissimilitude schemes to conduct steady-flow tests for the intake port. Through the reasonable combining of the two, the intake performance of the original engine was further improved. The results show that the valve structure has a relatively small influence on the intake mass, while it has a greater effect on the formation of the swirl in the cylinder, increasing the swirl ratio by 8.0%. The optimized valve structure model was combined with the valve lift dissimilitude scheme. It was found that the valve structure with optimal intake mass combined with the dissimilitude scheme of the largest valve lift of the spiral inlet could increase the flow coefficient by a maximum of 1.9%. The valve structure of the optimal swirl ratio combined with the dissimilitude scheme of the largest valve lift of the tangential inlet could increase the swirl ratio by a maximum of 9.7%. This study can guide diesel engines with combined intakes to increase the intake mass and improve the intake performance.

Keywords: Diesel engine; Combined inlet; Valve structural optimization; Valve lift dissimilitude; Intake performance.

NOMENCLATURE

CFD	Computational Fluid Dynamics	ST	valve lift dissimilitude combination of the spiral/tangential inlet
CI	Compress Ignition		
R	valve back arc	α	valve cone angle
R_S	valve back arc of the spiral inlet	$α_S$	valve cone angle of the spiral inlet
R_T	valve back arc of the tangential inlet	$α_T$	valve cone angle of the tangential inlet
SR	swirl ratio	γ	asterisk arm

1. INTRODUCTION

With the increasingly stringent regulations on fuel consumption and emission of motor vehicles, improving engine thermal efficiency and reducing engine emissions are the current research hotspots (Nath *et al*. 2021). The intake mass and in-cylinder gas flow state of the diesel engine directly affect the formation and combustion process of the fuel-air mixture in the cylinder (Guo *et al*. 2022; Malaiperumal *et al*. 2022). The intake valve is an important part of the intake system. Its structural parameters and valve lift will affect the flow

characteristics of the in-cylinder gas (Daniel *et al*. 2018; Indudhar *et al*. 2021). Therefore, optimizing the intake valve structure or using valve lift dissimilitude strategies can change the flow characteristics of the in-cylinder gas to improve the intake performance of the engine.

In recent years, many scholars have studied the influence of intake valve structure optimization and intake valve lift dissimilitude strategies on the gas flow characteristics in the cylinder. However, these researches were limited to improving the intake performance only through valve structure

optimization or valve lift dissimilitude strategies. In addition, most researchers adopted a single-parameter variable method to study the influence of valve structure on intake performance without considering the interaction between multiple structural parameters. Burak and Nureddin (2022) used CFD software to study the effect of different intake valve structures on the intake flow in diesel engines. They found that the valve structure would affect the flow velocity and direction of the gas entering the cylinder. By changing the critical geometric parameters of valves, such as fillet radius, cone angle, and seat angle, Maier *et al.* (2000) systematically studied the influence of intake valve structure on the port flow characteristics of the internal combustion engine using a single-parameter experimental method. They found that the valve cone angle and seat angle significantly affected the valve flow performance. Compared with a valve seat angle of 30°, when the valve seat angle was 40°, the swirl ratio of the middle valve lift was increased by 0.37. Due to the difference in the air intake modes, the pumping loss of the inlet injection throttleless spark ignition engine was significantly reduced at medium and low loads, but the combustion performance obviously deteriorated. Han *et al.* (2021) designed a spiral intake valve, which can form a vigorous swirl during the intake process. By measuring the intake swirl ratio and flow coefficient on a steady-flow port test bench, they proved that the spiral intake valve could generate a vigorous intake swirl when the opening lift was small (1-3 mm). When the spiral intake valve adopted the design scheme: 35° cone angle of the diversion hood, 55° spiral angle of the vane, and 8 long and 8 short vanes, the swirl ratio was significantly increased by 0.72 at 1 mm valve lift compared with the original engine scheme. In addition to the valve structure, controlling the opening and closing of the intake valve can also change the gas motion state in the cylinder (Arnau *et al.* 2021). A four-valve spark ignition engine had turbulent flow only when the two intake valves were fully opened. A vigorous swirl would be produced when one of the valves was closed, but the flow capacity was less than when the two intake valves were open (Cairns *et al.* 2013). In response to the problem of reducing the intake mass of a four-valve spark ignition engine to obtain a large-scale swirl in the cylinder, Kumar *et al.* (2021) put forward a variable dissimilitude lift method for the rotary valve. They used a fine rotary valve to enhance the swirl and changed the dissimilitude lift of the dual intake valves by adjusting the dissimilitude angle of the intake cam. Simulation and experimental results confirmed that the variable dissimilitude lift of the rotary valve could adjust the airflow motion in the cylinder without reducing the intake mass. Compared with the intake performance of the original diesel engine, when the dissimilitude angle was 8°, the swirl ratio can reach 0.51, increasing by 0.45, while the average flow coefficient was only reduced by 0.9%. At the maximum valve opening, the airflow motion between the dual inlets was seriously disturbed, which limited the flow coefficient and swirl ratio improvement. When the valve was at the maximum opening, the dissimilitude

valve schemes designed by Zhang *et al.* (2020) could make full use of the space in the cylinder so that the airflow in the cylinder formed a mutually staggered flow, avoiding serious interference of airflow between the inlets and realizing the improvement of the flow coefficient and swirl ratio. Compared with dual intake valves with the same valve lift of 12 mm, when the valve lift of the spiral/tangential intake ports was 12/8 mm, the maximum increase of swirl ratio was 11.4%.

At present, the main research trend is to enhance the swirl ratio through valve lift dissimilitude strategies on the one hand and to optimize the intake valve structure by a single structural parameter to improve the intake performance on the other hand. To further investigate the flow performance of valve structure and valve lift dissimilitude, this paper used computational fluid dynamics (CFD) numerical simulation and multi-parameter regression methods to optimize the dual intake valve structure, and three valve structures with better intake performance were obtained first. Then, the optimized intake valve structure model was combined with the valve lift dissimilitude scheme, and steady-flow testing was conducted for the intake port. The in-cylinder airflow movement was improved through the reasonable combining of the two, thereby further improving the intake performance.

2. STEADY-STATE EXPERIMENT AND SIMULATION MODEL VERIFICATION OF THE INTAKE PORT

2.1 Intake Port Steady-Flow Test Bench

(1) Establishment of the intake port steady-flow test bench

The engine intake port steady-flow test is the main research method to analyze the port-valve flow characteristics. According to the AVL intake port steady-flow test method (Jia *et al.* 2019a), an intake port steady-flow test bench was built, as shown in Fig. 1. The test bench consisted of 3D printed spiral and tangential intake ports, machined intake valves, a valve lift adjustment device, an electronic counter, a pressure sensor, a cylinder liner, a vane anemometer, a pressure stabilizer, a laminar flow meter, a diesel engine, and other components. The cylinder length employed in the test was 2.5 times of the cylinder diameter D, as recommended by AVL, and the swirl rotation measuring paddle was placed 1.75D below the top surface of the cylinder.

The test was conducted using a constant pressure differential method, i.e., keeping a constant pressure differential across the intake valve, and measuring the intake mass and the vane anemometer speed (n_{paddle}) at different valve lifts. The flow coefficient was calculated by the intake mass of the laminar flow meter, and the swirl ratio was calculated by the speed of the vane anemometer.

(2) Evaluation Indicators
The flow coefficient is the ratio of the actual air inflow to the theoretical air inflow in the cylinder
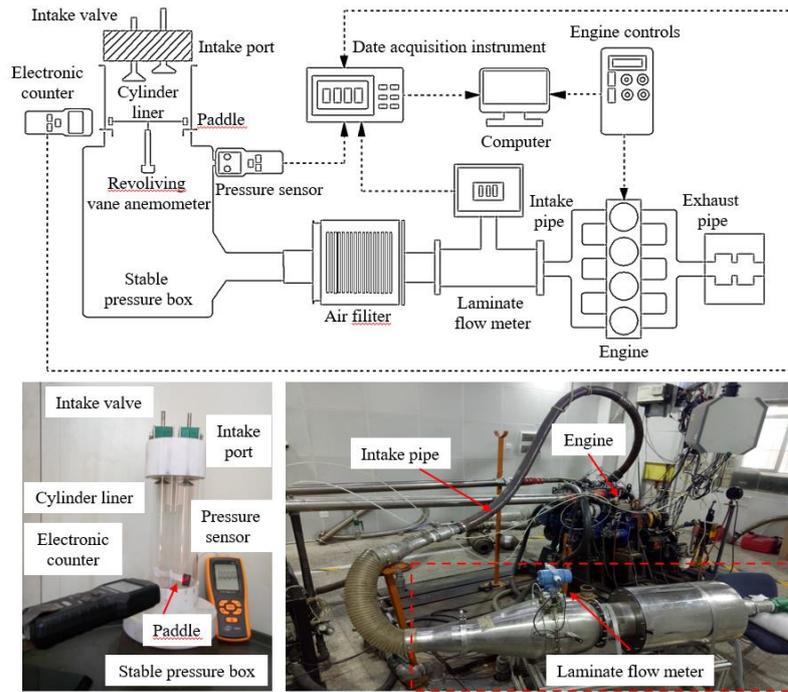
Fig. 1. Steady-flow bench for intake port testing.

(Galamboš *et al*. 2020). The swirl ratio is the specific value between the paddle speed in-cylinder and the engine speed. The equations for the flow coefficient and swirl ratio are as follows:

Flow coefficient equation:

$$\mu_\sigma = \frac{m_{actual}}{m_{theo}} = \frac{Q}{\rho A V_0} \tag{1}$$

$$V_0 = \sqrt{\frac{2\Delta_P}{\rho_m}} \tag{2}$$

Swirl ratio equation:

$$SR = \frac{n_{paddle}}{n_{engine}} \tag{3}$$

In the above equations, Q stands for the actual measured intake mass, kg/s; ρ stands for the air density, kg/m³; A stands for the effective flow area of the valve seat, m²; V_0 stands for the flow velocity into the cylinder, m/s; Δ_P stands for the actual pressure differential from inlet to outlet, Pa; ρ_m stands for the mean density from inlet to outlet, kg/m³; n_{paddle} stands for the vane anemometer speed, r/min; and n_{engine} stands for the engine speed, r/min.

2.2 Simulation Model and Verification

(1) Construction and verification of the transient flow model

To construct the CFD model, the maximum torque condition of the D19-type engine at 2200 r/min and 100% load was selected. The major parameters of the D19-type engine are shown in Table 1. The 3D solid model of the D19 engine was constructed as shown in Fig. 2 (a). The transient flow model of the D19 engine is shown in Fig. 2 (b). The initial and boundary conditions of the transient flow model are listed in Table 2.

Table 1 Major parameters of the D19-type diesel engine.

Item （Units）	Parameters
Engine type	Inline, four-stroke
Engine cylinder number	4
Valve number	16
Bore × stroke /mm	80×92
Compression ratio	18.5
Rated power /kW	82
Rated speed /r·min⁻¹	4000
Maximum torque /N·m	235
Speed /r·min⁻¹	1800-2300

(a) Solid model   (b) Mesh model
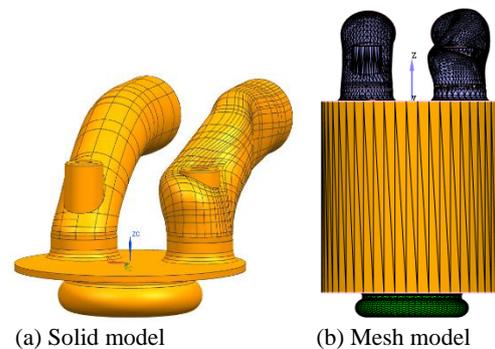
Fig. 2. Transient flow simulation model of the D19 engine.

Table 2 Initial and boundary simulation conditions of the transient flow model

Parameter	Numerical value	
Intake temperature/K	324	
Intake pressure/ kPa	176	
Piston surface temperature /K	550	
Cylinder temperature /K	450	
Cylinder head temperature /K	535	
Valve timing /crank angle	IVO	14°BTDC
	IVC	52°ABDC
	EVO	32.6°BBDC
	EVC	37.4°ATDC

The intake-to-compression process of the engine was simulated in this study. The simulated in-cylinder pressures were compared with the experimental values, which were derived from the literature Zhang *et al.* (2020). It can be seen from Fig. 3 (a) that the curves of the pressure in the cylinder of the simulated and the experimental value are in good agreement. In the engine bench test, the hourly intake mass of the engine was 201.1 kg/h, as measured by a laminar flow meter, and the simulated value was 200.6 kg/h. The difference between the two is 0.25%, as shown in Figs. 3 (a) and (b). The results show that the in-cylinder pressure and intake mass obtained from the numerical simulation agree with the experimental values. Therefore, the three-dimensional model and the initial and boundary conditions are accurate enough to satisfy the requirements of the simulation.

(a) Pressure
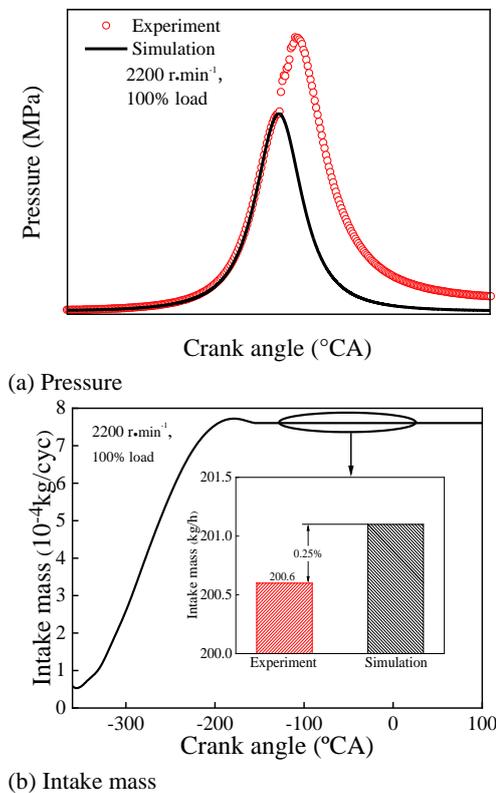
(b) Intake mass

Fig. 3. In-cylinder pressure and intake mass results from the simulation and experiments.
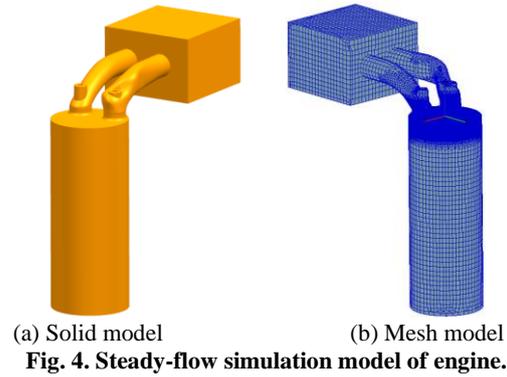
(a) Solid model   (b) Mesh model
Fig. 4. Steady-flow simulation model of engine.

(2) Construction and verification of the steady-flow model

In order to analyze intake port flow characteristics, a geometry model was developed. The model consisted of a rectangular stabilizing chamber for intake air pressure, two intake ports, two intake valves, two valve seats, and a cylinder, as shown in Fig. 4 (a). Automatic mesh generation was conducted using the AVL FAME Hybrid pretreatment function module for the ports (Jia *et al.* 2018). To accurately analyze the gas flow around the valve section, refining the mesh of the cylinder and the valve seat was necessary. The mesh of the solid model is shown in Fig. 4 (b). The mesh size is 0.3125-5mm, and the total number of cells is 810,000, with the hexahedral cells occupying approximately 90% of the total.

The intake process of the diesel engine follows the continuity equation of fluid motion, the law of conservation of momentum, and the conservation of energy. The Redlich-Kwong model was adopted for the gas flow equation (4) of the intake air (Lagarza Cortés *et al.* 2019). The Minmod Relaxation Difference scheme was used to solve the momentum conservation equation. The fluid in the model was compressible gas, which has a small-scale gas flow. Therefore, the RNG k-epsilon model was adopted for the turbulent motion of the intake air, as shown in equations (5) and (6) (Benajes *et al.* 2020). The test was conducted by using the constant pressure-differential method. The Cylinder wall boundary conditions used a standard wall function on the wall surface without slip, adiabatic, and fixed temperature values. The detailed parameters are shown in Table 3.

Gas flow equation:

$$PM = \rho RT \tag{4}$$

Turbulent model equation:

$$\frac{\partial(\rho\varepsilon)}{\partial t} + \frac{\partial(\rho\mu_j\varepsilon)}{\partial\chi_j} = -(\frac{2}{3}C_{\varepsilon1} - C_{\varepsilon3} + \frac{2}{3}C_\mu C_\eta \frac{k}{\varepsilon}\frac{\partial\mu_j}{\partial\chi_j})\rho\varepsilon\frac{\partial\mu_j}{\partial t} + \frac{\partial}{\partial\chi_j}(\frac{\mu_{eff}}{\sigma\varepsilon}\frac{\partial\varepsilon}{\partial\chi_j})$$
$$+\frac{\varepsilon}{k}[(C_{\varepsilon1} - C_\eta)\tau_{ij}\frac{\partial\mu_j}{\partial\chi_j} - -C_{\varepsilon2}\rho\varepsilon + C_S\dot{W}^s] \tag{5}$$

$$\frac{\partial(pk)}{\partial t} + \frac{\partial(p\mu_j\varepsilon)}{\partial t} = -\frac{2}{3}\rho k\frac{\partial\mu_j}{\partial\chi_j} + \tau_{ij}\frac{\partial\mu_j}{\partial\chi_j} + \frac{\partial}{\partial\chi_j}(\frac{\mu_{eff}}{\sigma k}\frac{\partial k}{\partial\chi_j}) - \rho\varepsilon + \dot{W}^s$$
$$+\frac{\partial}{\partial\chi_j}(\frac{\mu_{eff}}{\sigma k}\frac{\partial k}{\partial\chi_j}) - \rho\varepsilon + \dot{W}^s \tag{6}$$

Table 3 Initial and boundary simulation conditions of the steady-flow model.

Parameter	Numerical value
Altitude /m	1890
Inlet boundary pressure /kPa	81.6
Export boundary pressure /kPa	79.1
Intake air temperature /K	293
Turbulence length /m	0.001
Boundary kinetic energy /m²/s²	1
Gas flow equation	Redlich-Kwong
Turbulence model	RNG k-epsilon
Initial conditions	No wall slip, insulation

Fig. 5. Swirl ratio and flow coefficient comparisons between the simulation and experiment

In the above equations, n stands for the amount of substance, mol; R stands for the proportional coefficient, no unit; M stands for the molar mass of the gas, g/mol; ε stands for the turbulent dissipation rate in the cylinder, m²/s³; k stands for the turbulent kinetic energy in the cylinder, m²/s²; ρ stands for the mean density in the cylinder, kg/m³; μ stands for the dynamic viscosity of the fluid, N·s/m²; $C_{\varepsilon 1}$、$C_{\varepsilon 2}$、$C_{\varepsilon 3}$ and C_{η} are modified coefficients, no unit; $\dot{W}^{s}$ stands for the fluid compressibility, 1/Pa.

The simulated swirl ratio and flow coefficient were compared with that of the experimental values, and it was shown that the error is less than 5%, as shown in Fig. 5. The results indicate that the swirl ratio and flow coefficient obtained from the numerical simulation agree with the experimental values. Therefore, the three-dimensional model, initial, and boundary conditions are accurate enough to satisfy the requirements of the simulation.

3. INFLUENCE OF THE INTAKE VALVE STRUCTURE AND THE VALVE LIFT DISSIMILITUDE ON INTAKE PERFORMANCE

3.1 Influence of the Intake Valves Structure Optimization on Intake Performance

In the single-parameter study of the intake performance of the intake valve structure (Burak and Nureddin 2022), α and R are the valve structural parameters, where α stands for the valve cone angle, °; R stands for the radius of the valve back arc, mm. In this study, four key structural parameters of the intake valve were selected: the valve cone angle α_S and the valve back arc R_S of the spiral intake port; the valve cone angle α_T and the valve back arc R_T of the tangential intake port, as shown in Fig. 6.

(1) Experimental method and results of structural optimization of dual intake valves

Since the valve structure parameters are correlated with the number of experiments, the quadratic regression orthogonal rotation combined
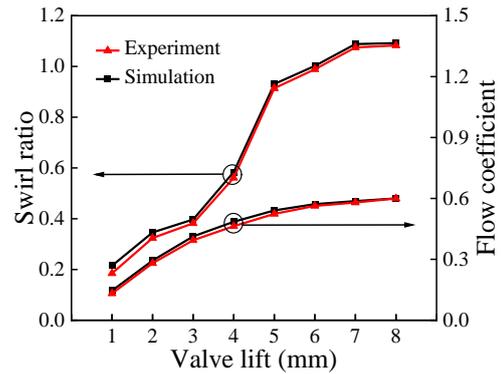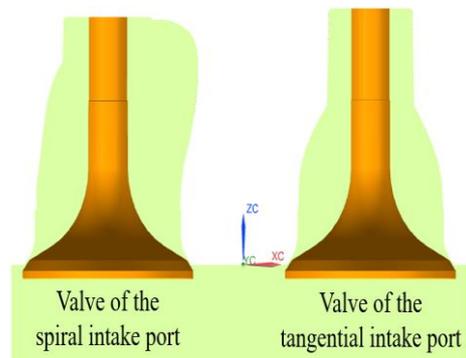
(a) Valve of the intake port
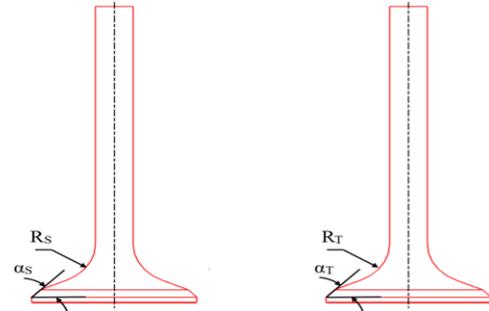
(b) Key structural parameters of the intake valve

Fig. 6. Spiral/tangential intake port valves and the key structural parameters.

experimental design method was used to optimize the structure of the dual intake valves. This method considers the interaction between various structural parameters, but allows the optimal experimental values to be determined quickly and accurately (Li *et al.* 2016).

The number of experimental factors in this study is m=4. γ is the asterisk arm, which refers to the distance from the center point. According to the quadratic regression orthogonal rotation combination design parameter table, the full implementation was chosen, then $\gamma=2$ (Li and Hu 2017). α_S, R_S, α_T, and R_T were defined as x_1, x_2, x_3, and x_4, respectively. The upper limit of α_L was

Table 4 Parameter level coding table of the experiment design.

Canonical variable (Z_j)	Variable (x_j)			
	x_1 /°	x_2 /mm	x_3 /°	x_4 /mm
Upper limit / γ	55	12	55	12
Upper level /1	50	10	50	10
Zero level /0	45	8	45	8
Lower level /-1	40	6	40	6
Lower limit /- γ	35	4	35	4
Variable spacing /$\triangle_j$	5	2	5	2

chosen as $x_{1\gamma}=55°$, the lower limit was $x_{1-\gamma}=35°$, and the zero level was $x_{10}=45°$. According to $\Delta_j = \dfrac{x_{j\gamma} - x_{j0}}{\gamma}$, the variable spacing was calculated as $\Delta_1=5°$, the upper level was $x_{11}=50°$, and the lower level was $x_{1-1}=40°$. Similarly, the codes for R_S, α_T, and R_T were calculated, as shown in Table 4.

The orthogonal combination design is composed of three experimental points. The experimental plans and results are shown in Table 5. Based on the quadratic regression orthogonal rotation combination table, 32 groups of experimental schemes were set up. The number of secondary-level experiments was $m_c=2^4=16$, and the orthogonal table L_{16} (2^{15}) was chosen for the transformation. The four factors are arranged in columns 1, 2, 4, and 7 in sequence; the number of asterisk tests is 2m=8. The last eight groups of experimental schemes were tested according to the orthogonal table L_9 (3^4). In Table 5, columns 2 to 5 from the left are the code value Z_j of the quadratic regression orthogonal combination design, columns 6 to 9 are the actual value X_j, and columns 10 and 11 are the experimental results.

For the calculation results of the 32 groups of experimental schemes, the quadratic regression

model Eq. (7) was used for the subsequent regression analysis. Then the approximate mathematical models among the intake mass, swirl ratio, and dual intake valve structural parameters were obtained, respectively.

$$y = a + \sum_{j=1}^{m} b_j x_j + \sum_{j<k} b_{jk} x_j x_k + \sum_{j=1}^{m} b_{jj} x_j^2 \qquad (7)$$

A quadratic regression analysis on the calculation results of the intake mass was carried out and obtained an approximate mathematical model Eq. (8) between the intake mass and the dual intake valve structure.

$$y = 0.79042 + 0.0004 Z_{13} + 0.0010 Z_{23} + 0.0011 Z_{24}$$
$$+(0.0034 - 0.0047 Z_1)Z_1 + (0.0001 - 0.0047 Z_2)Z_2$$
$$+(0.0005 - 0.0049 Z_3)Z_3 + (0.0001 - 0.0048 Z_4)Z_4 \qquad (8)$$

A quadratic regression analysis on the calculation result of the swirl ratio was carried out and obtained an approximate mathematical model Eq. (9) between the swirl ratio and the dual intake valve structure.

$$y = 1.19339 - 0.0007 Z_{13} + 0.0009 Z_{23} + 0.0007 Z_{24}$$
$$-(0.001 - 0.0046 Z_1)Z_1 + (0.0081 + 0.0079 Z_2)Z_2$$
$$-(0.0206 - 0.0074 Z_3)Z_3 - (0.0035 + 0.0023 Z_4)Z_4 \qquad (9)$$

Analyzing the regression Eq. (8), the p-values corresponding to the partial regression coefficients Z_1, Z_2, Z_3, and Z_4 are > 0.05, indicating that these partial regression coefficients are not significant for the intake mass regression equation. Therefore, it can be concluded that the key structures (α and R) of the intake valves of the spiral and tangential inlets have a small influence on the intake mass. For regression Eq. (9), the partial regression coefficient Z_2 p-value < 0.05, Z_3 p-value < 0.01, indicating that the partial regression coefficients Z_2 and Z_3 are significant for the swirl ratio regression equation. It can be seen that the valve back arc of the spiral inlet and the valve cone angle of the tangential inlet have a greater influence on the swirl ratio.
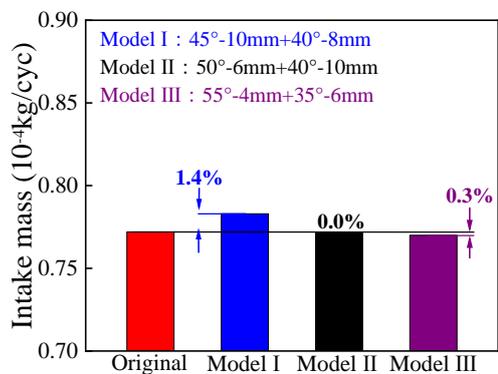
(a) Intake mass
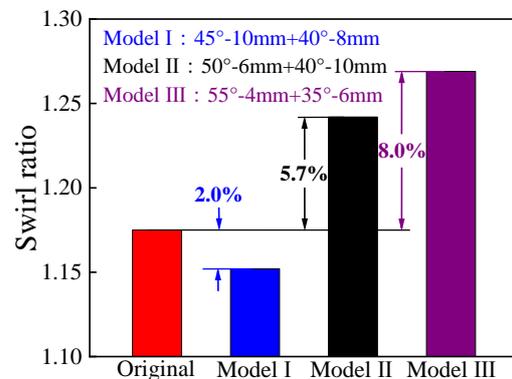
(b) Swirl ratio

Remarks: The data in the upper left of Fig.7 stands for the optimized structural parameters of the dual intake valves. They are the valve cone angle - the valve back arc of the spiral inlet's intake valve + the valve cone angle - the back arc of the tangential inlet's intake valve, respectively.

Fig. 7. Intake mass and swirl ratio after structure optimized of dual intake valves.

Table 5 Experimental schemes and results of valve structure optimization.

Schemes	Z_1	Z_2	Z_3	Z_4	x_1	x_2	x_3	x_4	y1 Intake mass/g	y2 Swirl ratio
1	1	1	1	1	50	10	50	10	0.778	1.167
2	1	1	1	-1	50	10	50	6	0.772	1.182
3	1	1	-1	1	50	10	40	10	0.771	1.253
4	1	1	-1	-1	50	10	40	6	0.771	1.253
5	1	-1	1	1	50	6	50	10	0.772	1.154
6	1	-1	1	-1	50	6	50	6	0.773	1.163
7	1	-1	-1	1	50	6	40	10	0.772	1.242
8	1	-1	-1	-1	50	6	40	6	0.773	1.204
9	-1	1	1	1	40	10	50	10	0.772	1.205
10	-1	1	1	-1	40	10	50	6	0.772	1.203
11	-1	1	-1	1	40	10	40	10	0.772	1.218
12	-1	1	-1	-1	40	10	40	6	0.772	1.240
13	-1	-1	1	1	40	6	50	10	0.773	1.167
14	-1	-1	1	-1	40	6	50	6	0.773	1.192
15	-1	-1	-1	1	40	6	40	10	0.772	1.188
16	-1	-1	-1	-1	40	6	40	6	0.770	1.219
17	γ	0	0	0	55	8	45	8	0.772	1.181
18	-γ	0	0	0	35	8	45	8	0.772	1.207
19	0	γ	0	0	45	12	45	8	0.772	1.232
20	0	-γ	0	0	45	4	45	8	0.772	1.195
21	0	0	γ	0	45	8	55	8	0.772	1.171
22	0	0	-γ	0	45	8	35	8	0.771	1.265
23	0	0	0	γ	45	8	45	12	0.772	1.158
24	0	0	0	-γ	45	8	45	4	0.772	1.175
25	0	0	0	0	45	8	45	8	0.774	1.178
26	-1	0	0	0	40	8	45	8	0.772	1.198
27	0	-1	0	1	45	6	45	10	0.772	1.177
28	0	0	1	-1	45	8	50	6	0.772	1.161
29	0	1	-1	0	45	10	40	8	0.783	1.152
30	1	-1	1	0	50	6	50	8	0.773	1.167
31	1	0	-1	1	50	8	40	10	0.772	1.228
32	1	1	0	-1	50	10	45	6	0.773	1.205
Original	-	-	-	-	48	8	48	8	0.772	1.175
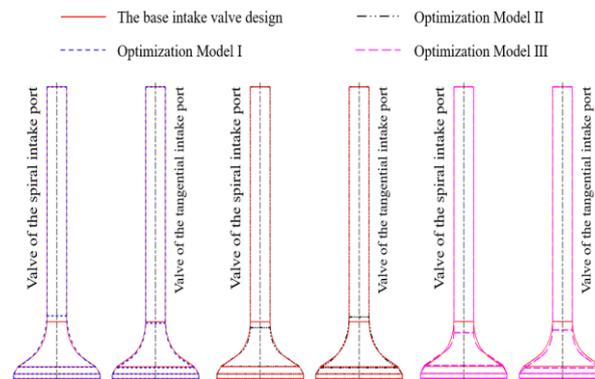
Fig. 8. Schematic diagram of key structural parameters of the optimized valve model.
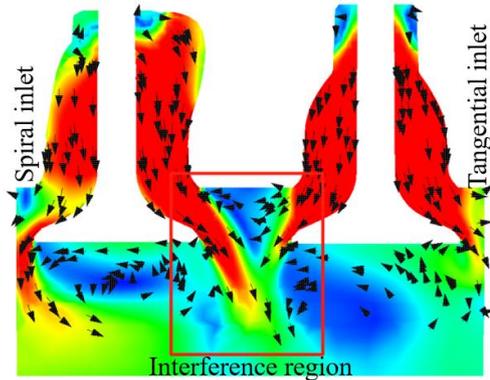
Fig. 9. Interference region of the intake flow.
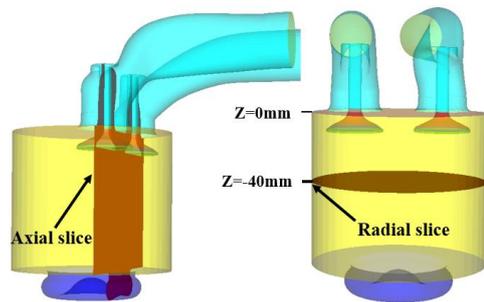
Fig. 10. Slice positions of the flow field .

From the above calculation results of the experiment schemes, the scheme with the largest intake mass was selected as the valve optimization model I. At this point, it can be concluded that the intake mass is increased by up to 1.4%, and the swirl ratio is reduced by 2%. The scheme with no loss of intake mass and the largest swirl ratio was selected as the valve optimization model II. For the approximate mathematical regression model of swirl ratio, the solver optimization tool was used to optimize the valve structures, and the scheme with the largest swirl ratio was selected as the valve optimization model III. The intake mass and swirl ratio of each valve optimization scheme is shown in Figs. 7 (a) and (b). Compared with the base valve, the changes in the key structural parameter of the optimized valve models are shown in Fig. 8.

(2) Flow field analysis of optimized valve structure

During the intake process, the airflow movement between the two valves of the spiral and tangential intake ports will interfere with each other in the cylinder, resulting in the loss of intake energy (Jia *et al.* 2019b), as shown in the red box area of Fig. 9. The intake valve has a guiding effect on the airflow. Optimizing the intake valve structure can change the flow direction of the intake air and reduce the interference of the airflow movement between the two intake ports. In order to intuitively analyze the influence of valve structure optimization on the flow field in the cylinder, the flow field slices shown in Fig. 10 were selected for analysis. The axial slices were taken along the central axis of the two valves, and the radial slices were taken radially 40 mm away from the cylinder head.

The velocity field and turbulent kinetic energy at the maximum opening of the intake valve were selected for analysis. The slice diagram is shown in Fig. 11. Compared with the original intake valve structure, the valve structure optimized model I increases the back arc of the spiral inlet valve, which improves the guiding effect of the airflow between the intake valve and the valve seat, and reduces the airflow passing resistance. At the same time, by reducing the valve cone angle of the tangential inlet, the airflow cross-sectional area becomes larger so that the intake resistance is reduced. Most of the air in the intake port flows into the cylinder along the area near the center line of the cylinder and moves to the bottom of the cylinder, and a small part of the air flows into the cylinder along the cylinder wall. At the same time, the turbulent kinetic energy distribution in the cylinder is concentrated. The intake flow velocity is the largest, reaching 135 m/s, and the intake mass is also the largest.

The valve structure optimization model II reduces the back arc of the spiral inlet valve and the cone angle of the tangential inlet valve. Under the premise of keeping the intake mass unchanged, the swirl ratio in the cylinder is maximized. The valve structure optimization model III reduces the back arc of the spiral inlet valve and the cone angle of the tangential inlet valve. The guiding effect of the valve structure changes the direction of the airflow entering the cylinder, reducing the intake flow interference in the adjacent area of the two intake valves and reducing the loss of intake energy. Most of the air in the spiral port flows into the cylinder radially, and a small part of the air flows into the cylinder along the cylinder wall. Most of the air in the tangential port flows tangentially into the cylinder, and a small part of the air flows into the bottom of the cylinder along the area near the center line of the cylinder. At the same time, the distribution area of turbulent kinetic energy in the cylinder is less and uniform. This benefits the swirl formation in the cylinder and improves the swirl ratio and turbulent kinetic energy. At this time, the turbulent kinetic energy in the cylinder is the largest, reaching 324 m^2/s^2.

3.2 Influence of the Valve Lift Dissimilitude on Intake Performance

(1) Experiment schemes of valve lift dissimilitude

When the valve lift is high, due to the large valve opening, a large amount of gas enters the cylinder, which significantly impacts the intake performance (Kubilay *et al*. 2019). Therefore, this section will focus on the maximum valve lift (8 mm) of the spiral and tangential inlets to study the influence of valve lift dissimilitude on the intake performance of the diesel engine. The experiment schemes are shown in Figs. 12 (a) and (b). ST is the combination of the valve lift dissimilitude for the spiral and tangential inlet. The maximum valve lift of the spiral inlet is defined as the dissimilitude scheme A, and the maximum valve lift of the tangential inlet is defined as the dissimilitude scheme B.
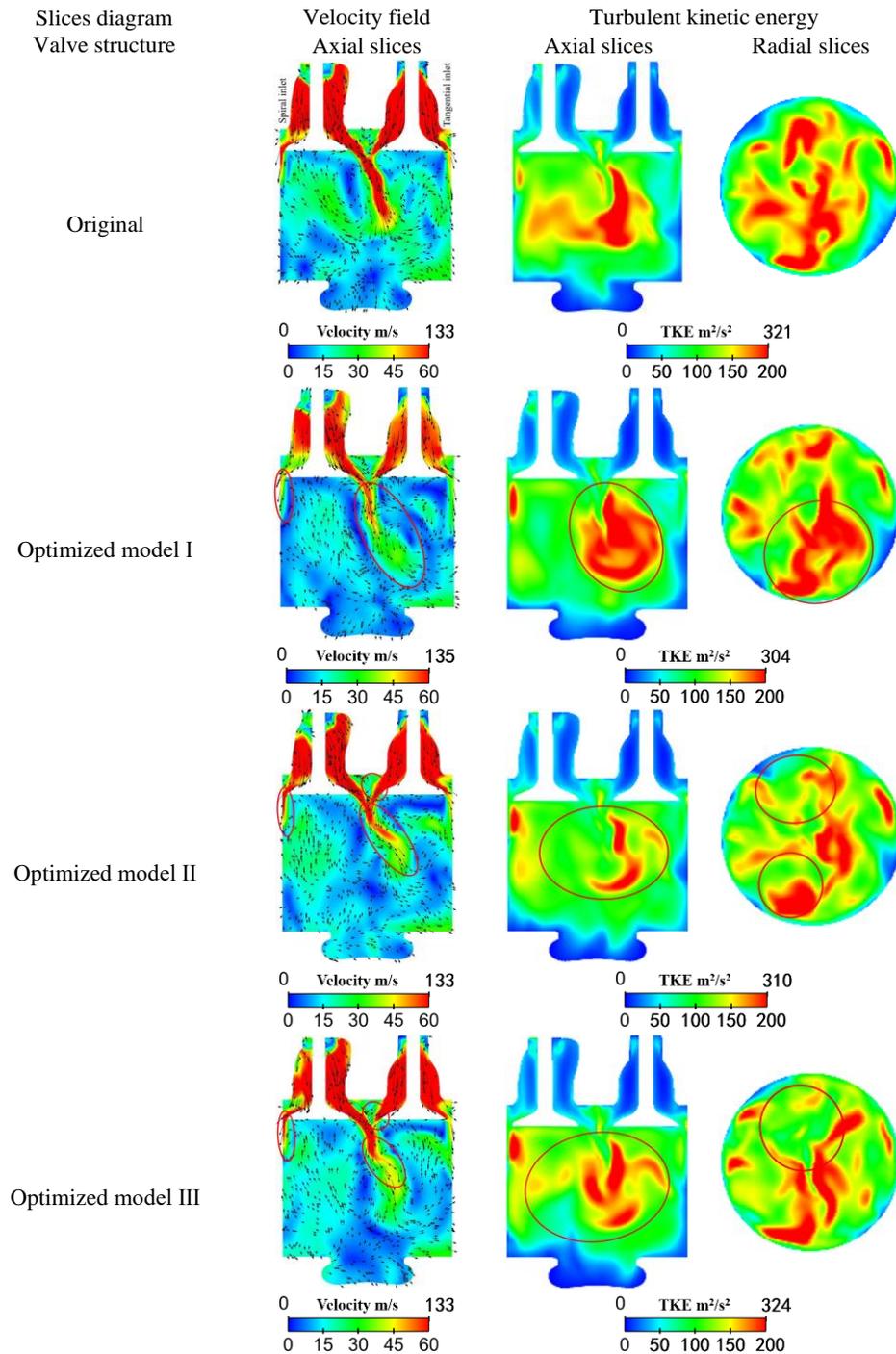
Fig. 11. Velocity field and turbulent kinetic energy field after valve structure optimization.

(2) Experiment results of valve lift dissimilitude

The results of the valve lift dissimilitude experiment of the two schemes are shown in Table 6. Compared with the intake performance of the original diesel engine with a valve lift of 6~8 mm, it can be concluded that the mean flow coefficient of scheme A increased by 1.5%, and the mean swirl ratio decreased by 3.5%. The mean flow coefficient of scheme B decreased by 0.7%, and the mean swirl ratio increased by 5.7%.

3.3 Influence of Optimized Valve Structure Models Combining Valve Lift Dissimilitude Schemes on Intake Performance

The differences in the intake valve structure and valve lift affect the intake performance of the diesel engine. The spiral and tangential inlets have different formation mechanisms for the in-cylinder swirl. The spiral inlet mainly relies on inlet spiral section-volute diversion to form an in-cylinder swirl, while the tangential inlet mainly relies on the airflow flowing

(a) ST 8/6

(b) ST 8/6.5

(c) ST 8/7

(d) ST 8/7.5

(a) The maximum valve lift of the spiral inlet

(e) ST 6/8

(f) ST 6.5/8

(g) ST 7/8

(h) ST 7.5/8
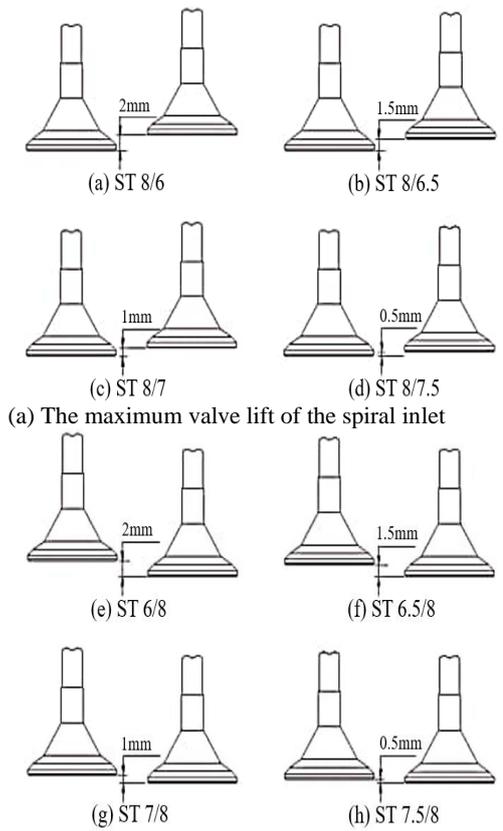
(b) The maximum valve lift of the tangential inlet
Fig. 12. Experimental schemes for valve lift dissimilitude of the spiral/tangential intake port

Table 6 Experimental results of spiral/tangential inlets valve lift dissimilitude

	Original	Scheme A	Scheme B
Mean flow coefficient	0.591	0.600	0.587
Mean swirl ratio	1.078	1.040	1.139

into the cylinder along the cylinder wall to form the swirl (Mohamed *et al.* 2017). Figure 13 (a) shows the velocity vector distribution in the cylinder when the valve lift dissimilitude is ST 8/6 mm in the original engine. When the valve lift of the spiral inlet reaches the maximum value, the valve lift of the tangential inlet decreases. The flow area between the valve seat and the valve becomes smaller, and the radial flow velocity of the air flowing out of the tangential inlet increases. Therefore, the airflow out of the tangential inlet intrudes into the side of the spiral inlet, destroying the intake swirl at the valve of the spiral inlet, thus affecting the formation of the intake swirl.

(1) Maximum valve lift of the spiral intake port

The intake performance experimental results of the valve lift dissimilitude of the optimized models I-III under the condition of the maximum valve lift of the spiral intake port are shown in Figs. 14 (a) and (b). As the valve lift dissimilitude of the two intake valves decreases, the swirl ratio increases. This is because the valve lift of the tangential intake port

(a) ST 8/6 valve lift dissimilitude
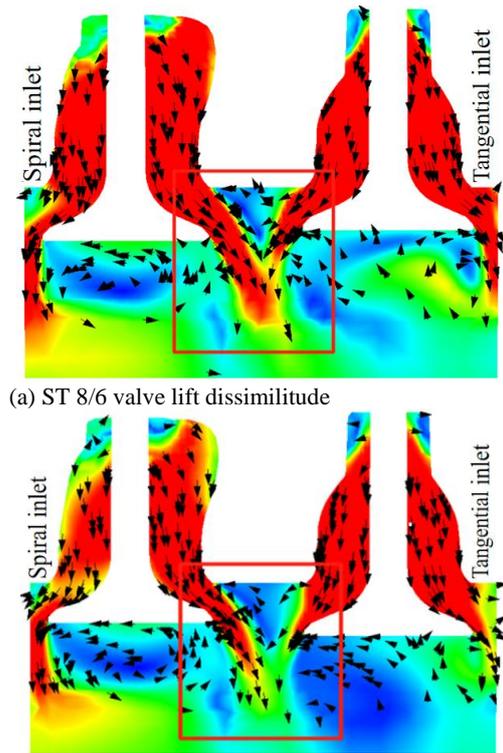
(b) ST 6/8 valve lift dissimilitude
Fig. 13. In-cylinder flow field of original engine with valve lift dissimilitude.
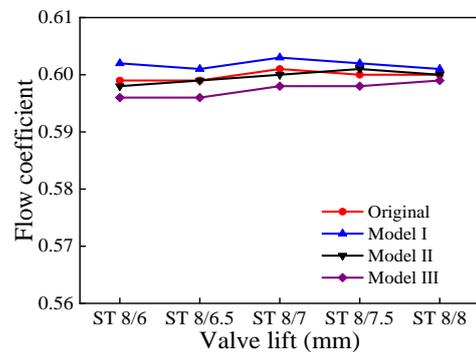
(a) Flow coefficient
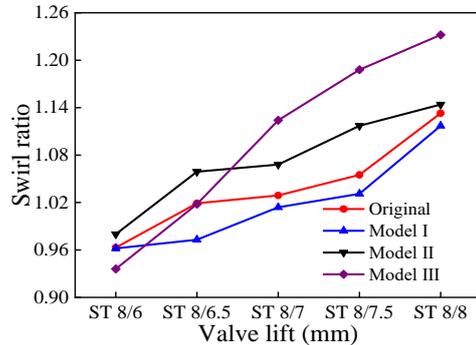
(b) Swirl ratio
Fig. 14. Flow coefficient and swirl ratio at valve maximum lift of spiral intake port.

increases, and the flow area of the intake air increases. The airflow velocity decreases, and the damage of the intake jet flow of the tangential inlet to the intake swirl of the spiral inlet is weakened. Compared with the intake performance of the

original diesel, the optimized valve structure combined with the valve lift dissimilitude further weakens the intake interference between the two intake valves. The flow coefficient of the valve structure optimized model I is better than the other structures. When the valve lift of the optimized model I is ST 8/6 mm, the maximum increase of the flow coefficient is 0.5%. Compared with the original diesel engine, when the valve lift of the optimized model III is ST 8/7.5 mm, the maximum increase of the swirl ratio is 12.6%.

(2) Maximum valve lift of the tangential intake port

Fig.13 (b) shows the velocity vector distribution in the cylinder when the original valve lift dissimilitude of the diesel engine is ST 6/8 mm. Under the maximum valve lift of the tangential intake port, the valve lift of the spiral intake port is reduced, so the valve lifts of the two intake valves are different. In this case, the airflow forms a staggered flow in the cylinder, avoiding the direct collision of the dual intake port airflow and improving the intake air interference to some extent. As shown in the variation curves in Fig. 15 (b), with the valve lift dissimilitude of the two intake valves decreasing, the in-cylinder swirl ratio increases first and then decreases, reaching a maximum value of ST 7/8 mm. When the opening of the spiral inlet valve is small (<7 mm), the swirl generation ability of spiral section-volute in inlets is not fully developed, and the swirl ratio is relatively small. When the two valves' lifts are the same, the swirl ratio will be reduced due to the interference of the tangential inlet intake jet flow. Compared with the intake performance of the original diesel engine, when the valve lift of the optimized model I is ST 7/8 mm, the maximum increase of the flow coefficient is 0.51%. When the valve lift of the optimized model III is ST 6/8 mm, the maximum increase of the swirl ratio is 6.0%.

(3) Experimental results of optimized valve structure models combining valve lift dissimilitude schemes

The optimized valve structure model was combined with valve lift dissimilitude schemes, and the experimental results are shown in Table 7. Compared with the intake performance of the original diesel engine, the valve optimized model I combines the valve lift dissimilitude scheme A, which can improve the flow coefficient by a maximum increase of 1.9%. The valve optimized model III combines the valve lift dissimilitude scheme B, which can improve the airflow movement in the cylinder, avoid intake air
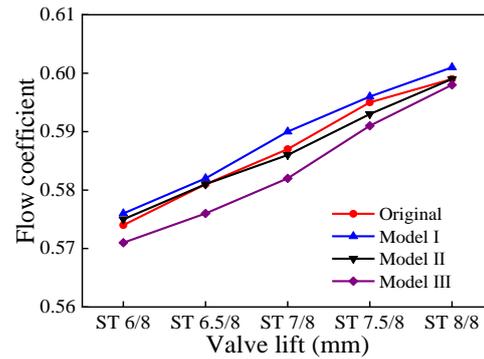
(a) Flow coefficient
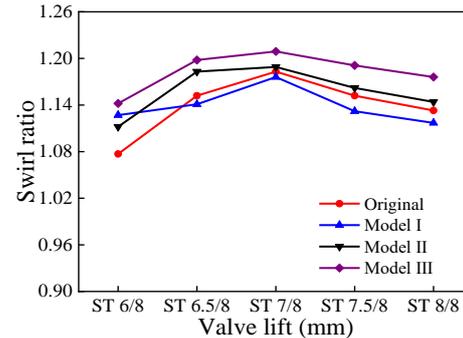
(b) Swirl ratio

Fig. 15. Flow coefficient and swirl ratio at valve maximum lift of tangential intake port.

interference, and improve the swirl ratio with a maximum increase of 9.7%.

4. CONCLUSIONS

This work studied the intake performance of the dual intake valve structure and valve lift dissimilitude in the CFD simulation model and steady-state experiment. Each valve structure and valve lift dissimilitude scheme has its own flow rule, and the reasonable combining of the two can further improve the intake performance. The following conclusions were drawn:

(1) For the optimization of the intake valve structure, the dual intake valve structure has less influence on the intake mass, which can only increase by 1.4%. However, the valve back arc of the spiral inlet and the valve cone angle of the tangential inlet have a greater influence on the swirl ratio, which can be increased by up to 8.0%.

Table 7 Experimental results of optimized valve structure combining valve lift dissimilitude

	Original	Structures / Lifts	Model I	Model II	Model III
Mean flow coefficient	0.591	Scheme A	0.602	0.600	0.597
		Scheme B	0.589	0.587	0.584
Mean swirl ratio	1.078	Scheme A	1.019	1.074	1.100
		Scheme B	1.139	1.158	1.183

(2) Under the condition of keeping the valve structure unchanged, compared with the intake performance of the original diesel engine, the flow coefficient can be increased by 1.5 % under the dissimilitude scheme A with a maximum valve lift of the spiral intake port. The swirl ratio can be increased by 5.7 % under the dissimilitude scheme B with a maximum valve lift of the tangential intake port.

(3) Compared with the intake performance of the original diesel engine, the flow coefficient can be increased by 1.9% when the optimal intake mass valve structure is combined with the dissimilitude scheme of the maximum valve lift of the spiral intake port. The maximum swirl ratio can be increased by 9.7% when the optimal swirl ratio valve structure is combined with the dissimilitude scheme of the maximum valve lift of the tangential intake port.

ACKNOWLEDGEMENTS

REFERENCES

Arnau, F. J., J. Martín, B. Pla and Á. Auñón (2021). Diesel engine optimization and exhaust thermal management by means of variable valve train strategies. *International Journal of Engine Research* 22(4), 1196-1213.

Benajes, J., R. Novella, J. Gómez-Soriano and I. Barbery (2020). Computational assessment towards understanding the energy conversion and combustion process of lean mixtures in passive pre-chamber ignited engines. *Applied Thermal Engineering* 178, 115501.

Burak, S. and D. Nureddin (2022). Numerical investigation of the effects of intake valve geometry on air flow during intake stroke. *International Journal of Energy for a Clean Environment* 23(1), 39-51.

Cairns, A., H. Zhao, A. Todd and P. Aleiferis (2013). A study of mechanical variable valve operation with gasoline-alcohol fuels in a spark ignition engine. *Fuel* 106, 802-813.

Daniel, B., S. Adrian and C. Rui (2018). Influence of asymmetric valve strategy on large-scale and turbulent in-cylinder flows. *International Journal of Engine Research* 19(6), 631-642.

Galamboš, S. L., N. M. Nikolić, D. A. Ružić and J. Ž. Dorić (2020). An approach to computational fluid dynamic air-flow simulation in the internal combustion engine intake manifold. *Thermal Science* 24, 127-136.

Guo, Y. Z., H. L. Kui, C. S. Shao and Z. Z. Wang (2022). Flow characteristics of a Dual-Intake Port Diesel Engine with Guide Vanes. *Journal of Applied Fluid Mechanics* 15(3), 709-722.

Han, K., Y. J. Chang, Z. F. Xie and P. Fang (2021). Structure optimization of helical valve and its influence on combustion performance of an unthrottled SI engine. *Automotive Engineering* 43(1), 27-33.

Indudhar, M. R., N. R. Banapurmath, K. G. Rajulu and A. Y. Patil (2021). Optimization of piston grooves, bridges on cylinder head, and inlet valve masking of home-fueled diesel engine by response surface methodology. *Sustainability* 13(20), 11411.

Jia, D. W., X. W. Deng and J. L. Lei (2018). Steady-state experiment and simulation of intake ports in a four-valve direct injection diesel engine. *Journal of Applied Fluid Mechanics* 11(1), 217-224.

Jia, D. W., X. W. Deng and J. L. Lei (2019a). Intake flow interference analysis of combination intake port in diesel engine. *Journal of Applied Fluid Mechanics* 12(1), 61-67.

Jia, D. W., X. W. Deng, Y. Wang and J. L. Lei (2019b). Flow field influence analysis of combination intake port to port and in-cylinder for a four-valve diesel engine. *Journal of Applied Fluid Mechanics* 12(3), 871-881.

Kubilay, B., Y. Semih and D. Kerim (2019). Numerical investigation of valve lifts effects on performance and emissions in diesel engine. *International Journal of Global Warming* 18(3-4), 287-303.

Kumar, P., A. Darsigunta, B. C. Mouli and V. K. Sharma (2021). Analysis of intake swirl in a compression ignition engine at different intake valve lifts. *Materials Today: Proceedings* 47, 2869-2874.

Lagarza Cortés, C., J. Ramírez-Cruz, M. Salinas-Vázquez and W. Vicente-Rodríguez (2019). Large-eddy simulation of transcritical and supercritical jets immersed in a quiescent environment. *Physics of Fluids* 31(2), 025104.

Li, T., Y. Jia and S. Liu (2016). Optimizing conditions to induce artificial gynogenesis in Culter alburnus using a quadratic orthogonal rotation design. *Journal of Fishery Sciences of China* 23(01), 77-89.

Li, Y. Y., and C. R. Hu (2017). Experiment design and data processing. Beijing: Chemical Industry Press, 217-238.

Maier, A., T. H. Sheldrake and D. Wilcock (2000). Geometric parameters influencing flow in an axisymmetric IC engine inlet port assembly: Part II—parametric variation of valve geometry. *Journal of Fluids Engineering* 122(4), 658-665.

Malaiperumal, V., C. G. Saravanan, V. Raman and R. K. Kirubagaran (2022). Effect of intake port

design modifications on diesel engine characteristics fuelled by pine oil-diesel blends. *Energy Sources, Part A: Recovery, Utilization, and Environmental Effects* 1-17.

Mohamed, A. E. S., S. Abo-Elfadl and A. E. M. M. Nassib (2017). Effect of shroud and orientation angles of inlet valve on flow characteristic through helical–spiral inlet port in diesel engine. *Journal of Engineering for Gas Turbines and Power* 139(10), 1-7.

Nath, T. V., P. Shrivastava, U. Rajak and G. Dwivedi (2021). A comprehensive review of the influence of physicochemical properties of biodiesel on combustion characteristics, engine performance and emissions. *Journal of Traffic and Transportation Engineering* 8(4), 510-533.

Zhang, W., Y. X. Wang, Y. Y. Peng and Z. H. Chen (2020). Steady flow test and combustion analysis of different spiral/tangential air-passage valves. *Automotive Engineering* 42(11), 1537-1544.